Aerospace Science and Technology, 1998, n° **1**, 37-47

Linear Stability Analysis in Transonic Diffuser Flows

G. Casalis, J.-Ch. Robinet

ONERA-CERT, 2, avenue Edouard Belin, F 31055 Toulouse Cedex.

Manuscript received November 21, 1996; accepted May 30, 1997.

Casalis G., Robinet J.-Ch., *Aerospace Science and Technology*, 1998, n° **1**, 37-47.

Abstract

The purpose of this paper is to give the first results of a linear stability analysis which has been applied to the problem of shock oscillations in a transonic diffuser flow. The mean flow is calculated with a numerical code solving the averaged Navier-Stokes equations, but the proposed stability approach is limited to the core region where the viscous effects can be neglected. In order to validate the present approach, the results are compared with Sajben's experimental results and those numerically obtained by Liou and Coakley. It is the first time that these published results are compared with a simple linear stability analysis. As demonstrated below, the shock motion spectra have been correctly reproduced and the frequencies of 200 Hz and 300 Hz have been clearly obtained for the diffuser lengths of $l/h = 13$ and $l/h = 8.6$ respectively. As far as stability of the mean flow is concerned, the temporal amplification rate is always negative, the mean flow is therefore linearly stable. Finally, the amplitude and phase of the fluctuating pressure have been compared. The phase for example is in very good agreement with the experimental results. This can prove that at least in some cases, self-sustained shock oscillations can be explained and predicted with an inviscid linear stability analysis. © Elsevier, Paris

Keywords: Stability – Shock oscillations – Diffuser.

Résumé

Une analyse de stabilité linéaire dans un écoulement de tuyère transsonique. L'objectif de ce papier est de donner les premiers résultats d'une analyse de stabilité linéaire appliquée au problème d'oscillation de choc dans un écoulement de tuyère transsonique. L'écoulement moyen est calculé grâce à un code numérique résolvant les équations de Navier-Stokes moyennées. L'analyse de stabilité est limitée à la zone de l'écoulement où les effets visqueux peuvent être négligés. Afin de valider cette approche, les résultats obtenus sont comparés à des résultats issus des expériences de Sajben ainsi qu'à ceux obtenus numériquement par Liou et Coakley. C'est à notre connaissance la première fois que ces résultats publiés sont comparés à une analyse de stabilité. Il est monté que, le spectre de déplacement du choc a été correctement reproduit et en particulier les fréquences de 200 Hz et 300 Hz ont été clairement obtenues respectivement pour des longueurs de tuyère de $l/h = 13$ et $l/h = 8.6$. En ce qui concerne la stabilité de l'écoulement moyen, le coefficient d'amplification temporelle est toujours négatif, ce qui en garantie la stabilité linéaire. Pour finir, l'amplitude et la phase de la fluctuation de pression ont été comparés avec les résultats publiés. La phase, par exemple, est en très bon accord avec les résultats expérimentaux. Ces comparaisons montrent qu'au moins dans certains cas, les oscillations de choc auto-entretenues peuvent être expliquées et prédites grâce à une simple analyse de stabilité linéaire non visqueuse. © Elsevier, Paris

Mots-clés : Stabilité – Oscillation de choc – Tuyère.

NOMENCLATURE

k	wave number
$\omega/2\pi$	frequency
U, u	streamwise velocity component
V, v	vertical (transverse) velocity component
T	temperature
ρ	density
$\mathbf{Z}$	fluctuation vector (U, V, ρ, T)
t	time
X	amplitude of the shock motion
Rp	exit pressure to total inlet pressure ratio
l	diffuser length (from throat to exit)
h	throat height

Subscripts

$(\ )_r$	real part
$(\ )_i$	imaginary part
$(\ )_f$	fluctuation value
$(\ )_c$	shock value
$(\ )_1$	downstream value
$(\ )_0$	upstream value
$(\ )_u$	uniform zone value
$(\ )_e$	exit value

Superscripts

$\overline{(\ )}$	mean value

I – INTRODUCTION

For performance reasons, some engines are built nowadays with over-relaxed diffusers. However, it has now been established that in some configurations such diffusers may exhibit self-sustained oscillations which constitute major limitations in vehicle performance. Depending on different parameters such as the diffuser geometry, the inlet/exit pressure ratio and the upstream Mach number, different phenomena can occur. The most important characteristics are the occurrence and size of a separation bubble just behind the shock and oscillation of the shock position as well as of the whole downstream flow.

The purpose of this paper is to present a new approach initiated at ONERA-CERT in the Aerothermodynamics Department. This approach consists in studying these oscillations using a simple linear stability analysis based on the classical general small perturbation technique. However the analysis is restricted to the core region, even if the averaged flow is calculated using the complete Navier-Stokes equations. In effect, the mean flow computation has been performed with the "FLU3M" code developed at ONERA (OAal) [1].

The first part discusses the publications forming the background of this study. In the second part, the theoretical aspects of the present approach and the numerical procedure are detailed. Finally, the stability results are shown in comparison with Sajben's experiments and with Liou and Coakley's numerical simulations.

II – BACKGROUND OF THE PRESENT STUDY

II.1 – Diffuser geometry

In the beginning of the 1980's, a McDonnell Douglas team, headed by M. Sajben experimentally studied shock-wave oscillation in a transonic diffuser flow [2-4] under natural conditions.

Sajben *et al.* have used different diffuser types, essentially two diffuser models labelled G and B according to Sajben's terminology. All diffuser have a rectangular section; they are asymmetric with a flat bottom wall and a converging-diverging channel with a maximum 9° divergence angle as top wall. The diffuser is equipped with many suction slots, so that the flow can be considered to be two-dimensional, at least in the middle of the side walls of the channel. A diagram of the G diffuser model is shown in *Figure* 1. The present paper is limited to results for type G. The relative length of the diffuser is $l/h = 13$ where h is the height at the throat.

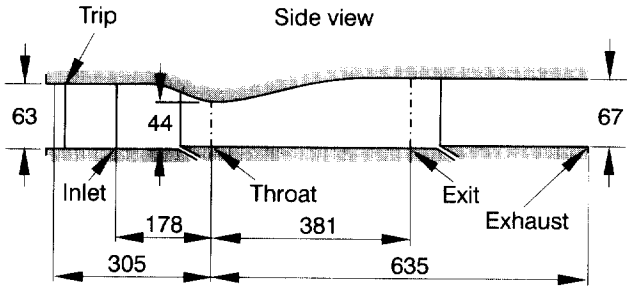

Fig. 1. – Diffuser model type G.

II.2 – General descriptions

In these experimental studies, the fluid accelerates from subsonic to supersonic speed through a sonic throat, and is abruptly decelerated by a shock-wave located downstream of the throat. The flow conditions are essentially characterised by the ratio of the static pressure at the exit to the total pressure at the inlet: $Rp = p/pt$. This ratio determines, among other properties, the shock strength and the upstream Mach number M_0. The following results are limited to one value of Rp: $Rp = 0.72$, which corresponds to the most detailed published results.

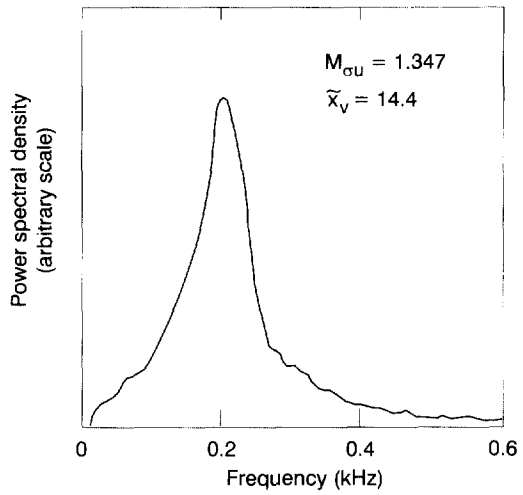

Fig. 2. – Shock motion power spectrum, experiment.

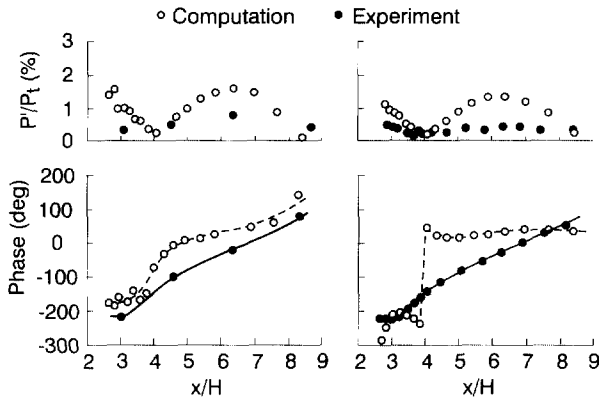

Fig. 3. – Comparisons of pressure fluctuation amplitude (top) and phase (bottom); left: top wall, right: core flow.

II.3 – Experimental results

Under some conditions, which depend on the value of Rp, the flow exhibits natural oscillations with a well-defined frequency. These oscillations consist of a shock motion and of the occurrence of oscillations downstream of the shock. However, no oscillations have been observed in the supersonic zone.

The shock motion power spectrum represented in *Figure* 2, taken from [2], which has been filtered between 100 and 300 Hz, shows that the most sensitive frequencies are close to 200 Hz in this case.

Another interesting result is given by the streamwise variation of the pressure fluctuation. Sajben *et al.* have shown that the amplitude of the pressure fluctuation remains almost constant whereas its phase clearly increases with respect to x. *Figure* 3, taken from [8], shows this variation of the pressure fluctuation in the core flow and also near the top wall. In this figure, the experimental results (closed symbols) correspond to natural oscillations.

II.4 – Numerical simulations

In the middle of the 1980's, many numerical simulations were made by Liou and Coakley's team using the same configurations as Sajben's [5-8]. These simulations consisted in computing the unsteady averaged Navier-Stokes equations with a classical turbulence model. They were achieved in two steps: steady computations give the mean flow and then the unsteady ones gave the variation of the fluctuating quantities. The authors investigated the same quantities as in the experiments: among other things, the shock motion power spectral density distribution and the amplitude and phase of pressure fluctuation. In reference [7], Hsieh *et al.* studied many diffuser lengths: l/h = 8.66 (case A), 10.06 (case B), 12.08 (case C) and 14.77 (case D). As indicated in *Figure* 4, taken from [7], the location of the downstream boundary has a strong effect on the frequency of the self-excited oscillation in the transonic diffuser flow. The oscillation frequency reduces from 300 to 210 Hz as the downstream boundary varies from l/h = 8.6 to 12.08. This means that the frequency reduces as the length of the diffuser decreases. For the greatest length: l/h = 14.7, the trend is reversed: the frequency of oscillation increases to 310 Hz. According to the authors, these results suggest that the mechanism causing the self-excited oscillation changes from cases dominated by a viscous and convective wave (A, B and C) to a case dominated by an inviscid acoustic wave (D).

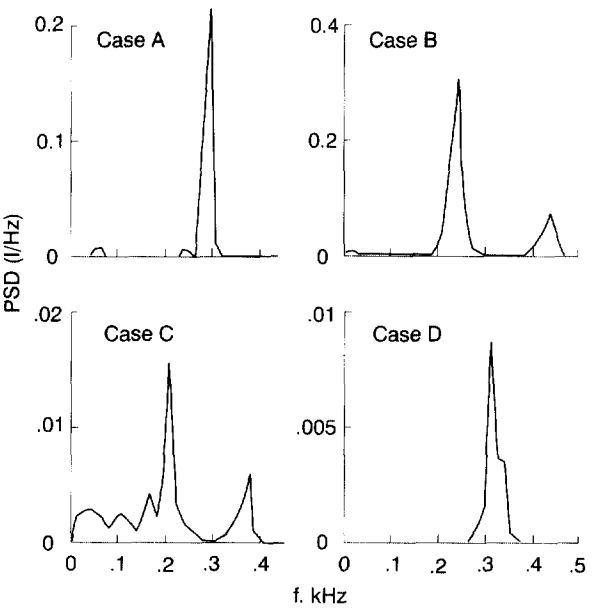

Fig. 4. – Power spectrum density distribution: different diffuser lengths.

On the other band, with regard to the computed amplitude and phase of the pressure fluctuation, which have been plotted in *Figure* 3 (open symbols),

a major difference appears between amplitude of fluctuation is significantly higher than the experimental one. Moreover pressure nodes are observed for $x/h = 4$ and $x/h = 8.5$, whereas unforced experimental diffusers do not present any nodes. But the greatest difference between calculation and experiment concerns the phase. The experimental phase in the core flow increases whereas the numerical phase is not monotonic and exhibits a jump at $x/h = 4$.

Taking into account all these published results, which are not fully understood, a new approach based on the linear stability theory has been developed in the Aerothermodynamics Department of ONERA-CERT. The objectives are first to give a physical explanation for the observed shock oscillations, and secondly to compare the stability results with Sajben's experimental ones and with those numerically obtained by Liou and Coakley.

III - THEORETICAL ASPECTS

III.1 - Basic equations

The proposed stability theory is based on the classical small perturbation technique. All the physical quantities q (velocity, pressure...) are decomposed into a mean value and a fluctuating one:

$$q = \bar{q} + q_f. \tag{1}$$

The physical quantities related to the mean flow are overlined; for example, $\overline{U}$ is the mean streamwise velocity component.

Emphasis must be given to the different types of flow: the mean flow comes from the Navier-Stokes equations while the viscous terms will be neglected in the stability equations.

The mean Navier-Stokes flow has been computed by ONERA with the FLU3M code. The condition are given by the pressure ratio $Rp = 0.72$ and by the diffuser length $l/h = 13$. In order to compare the stability results with the computations of Liou, another length ($l/h = 8.6$) will be considered below. In the shorter case, the corresponding mean flow will be simply the previous one truncated. In effect, in the core region, the mean flow is nearly constant from $x/h = 5$ to the exit section.

Let us now give the general equations for the instantaneous flow denoted by variable q in equation (1). The two-dimensional diffuser is considered with the usual coordinate system (x, y). The x axis refer to the principal direction of the diffuser and y is perpendicular to it. The equations of motion for the instantaneous flow are the Euler equations, the energy equation written for the total enthalpy and the equation of state of perfect gas.

- Equation of continuity:

$$\frac{\partial \rho}{\partial t} + \frac{\partial (\rho U)}{\partial x} + \frac{\partial (\rho V)}{\partial y} = 0 \tag{2}$$

- x-momentum equation:

$$\frac{\partial U}{\partial t} + \rho U \frac{\partial U}{\partial x} + \rho V \frac{\partial U}{\partial y} + \frac{\partial P}{\partial x} = 0 \tag{3}$$

- y-momentum equation:

$$\rho \frac{\partial V}{\partial t} + \rho U \frac{\partial V}{\partial x} + \rho V \frac{\partial V}{\partial y} + \frac{\partial P}{\partial y} = 0 \tag{4}$$

- Enthalpy equation:

$$\rho \frac{\partial h_i}{\partial t} + \rho U \frac{\partial h_i}{\partial x} + \rho V \frac{\partial h_i}{\partial y} + \frac{\partial P}{\partial t} \tag{5}$$

- Total enthalpy definition:

$$h_i = C_p T + \frac{1}{2}(U^2 + V^2) \tag{6}$$

- Equation of state:

$$P = \rho r T. \tag{7}$$

The instantaneous shock equations are the Rankine-Hugoniot relations:

$$\rho_1 (V_{n1} - W_c) = \rho_0 (V_{n0} - W_c) \tag{8}$$

$$P_1 + \rho_1 (V_{n1} - W_c)^2 = P_0 + \rho_0 (V_{n0} - W_c)^2 \tag{9}$$

$$V_{\tau 1} = V_{\tau 0} \tag{10}$$

$$C_p T_1 + \frac{1}{2}(V_{n1} - W_c)^2 = C_p T_0 + \frac{1}{2}(V_{n0} - W_c)^2 \tag{11}$$

where V_n is the velocity component normal to the shock, V_τ is the parallel component and W_c is te velocity of the shock front.

III.2 - Mean flow calculation

Before describing the stability theory in detail, the first step is to check that the computed mean flow is in agreement with Sajben's experimental results. *Figures* 5 and 6 show the experimental and numerical results respectively for the iso-$\overline{U}$ contours.

Other comparisons concerning other mean quantities are given in [9]. From these result, it can be concluded without any doubt that the computed mean flow, the stability of which is discussed below, is in very good agreement with the experimental data.

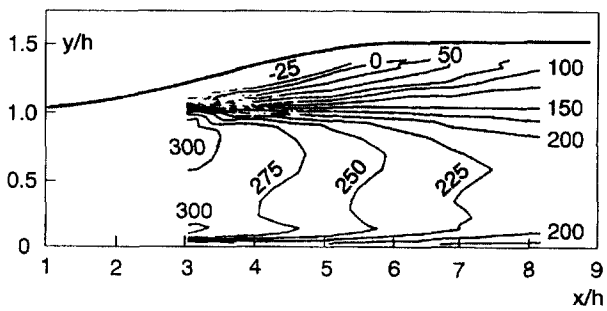

Fig. 5. - Mean $\overline{U}$ contours (m/s), experiment.

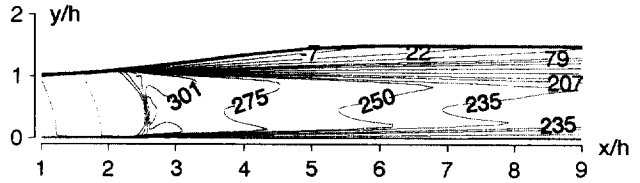

Fig. 6. – Mean $\overline{U}$ contours (m/s), calculation.

III.3 – Stability theory

III.3.1 – *Mathematical form of the perturbation*

The decomposition (1) is introduced in equations (2) to (7). The latter are written in the core region. Therefore, it must be assumed that the mean flow, which satisfies the Navier-Stokes equations, is also a solution of these inviscid equations. The resulting equations are further simplified by considering that the perturbation is small, so that the nonlinear fluctuating terms can be neglected.

Finally, equations (2) to (7) are transformed into a linear system, whose coefficients are a function of the mean flow. This mean flow is clearly independent of time t. Furthermore, according to the experimental and numerical results (see *Figs.* 5 and 6), the mean flow can be assumed to be weakly dependent on y, so that any mean quantity verifies the relation:

$$\partial\bar{q}/\partial y \ll \partial\bar{q}/\partial x \quad \forall\, x, \forall\, y. \tag{12}$$

This quasi-one-dimensionality allows us to simplify the equations again, writing the perturbation in a wave-like form:

$$q_f(x, y, t) = \mathfrak{Re}\left[q(x) \cdot e^{i(ky-\omega t)}\right], \tag{13}$$

where k is a wave number, $\omega/2\pi$ the frequency of the perturbation and $\mathfrak{Re}(z)$ the real part of z. In this paper, only the case with k real and ω complex is considered. The present approach corresponds to the so-called temporal theory. Finally, the fluctuating quantities are written as:

$$q_f(x, y, t) = \mathfrak{Re}\left[q(x) \cdot e^{\omega_i t} \cdot e^{i(ky-\omega_r t)}\right], \tag{14}$$

where the imaginary part ω_i of ω is a temporal amplification coefficient. The physical meaning of ω_i is in accordance with the classical definition of stability. In effect, when $\omega_i > 0$ the mean flow is unstable whereas for $\omega_i < 0$ the mean flow is stable.

III.3.2 – *Linearised Euler equations*

With the mathematical form (14) for the fluctuation, the linearised Euler equations lead to an ordinary fourth-order differential system:

$$\mathbf{C}\frac{d\mathbf{Z}}{dx} = \mathbf{B}\mathbf{Z}, \tag{15}$$

where $\mathbf{Z}$ stands for (T, ρ, u, v). $\mathbf{Z}$ is the amplitude function vector of the perturbation and $\mathbf{C}$ and $\mathbf{B}$ are two (4×4) matrices with complex coefficients which are functions of the mean flow and the coefficients ω and k. Their analytical expressions are given in the Appendix (A1 and A2).

III.3.3 – *Boundary conditions*

In all the experimental configurations tested, no fluctuation has been observed at the throat. For this reason, the first boundary condition simply states:

$$\mathbf{Z}(0) = 0. \tag{16}$$

This condition has to be postulated as it cannot be demonstrated.

In the exit section, the fluctuations do not necessarily vanish. We only impose that the perturbations remain finite at this exit section:

$$\mathbf{Z}(l/h) \text{ is bounded.} \tag{17}$$

III.4 – Discussion

III.4.1 – *Eigenvalue problem*

The trivial solution $\mathbf{Z} \equiv 0$ is obviously a solution of the stability problem (15)-(17). Moreover, it is the only one unless this stability problem becomes singular. Equations (15) with boundary conditions (16) and (17) therefore appear as a generalised eigenvalue problem.

By calculating the determinant of matrix $\mathbf{C}$ (Appendix A1), it is straightforward to prove that matrix $\mathbf{C}$ is always invertible except at the mean shock position ($\overline{M}^2 = 1$). The first consequence of this is deduced from equation (15) and boundary condition (16): **there is no fluctuation in the supersonic zone** (from throat to shock). However, the system of equations (15) is singular at the shock: another solution, different from the trivial solution, may exist! To find a non-zero solution, a special procedure must be established at the shock position. Coming back to the physics, this procedure can be clearly obtained with the shock equations (8) to (11). The following section is devoted to this special treatment.

III.4.2 – *Linearised Shock equations*

The same small perturbation technique (1) is used for the shock equations. For example, the perturbed position of the shock is written as:

$$x = \bar{x}_c + \mathfrak{Re}\left[X\, e^{i(ky-\omega t)}\right], \tag{18}$$

where $\bar{x}_c$ is the mean shock position and X represents the shock oscillation amplitude. X is assumed to be a small quantity. The Rankine-Hugoniot equations are then linearised by performing a first order Taylor expansion with respect to X. The quantities downstream of the shock are denoted by subscript 1 and those upstream of the shock by subscript 0. For example, q_1 is the value of the quantity q, itself the sum of the mean and fluctuating quantities evaluated just downstream of the perturbed position of the shock. q_1 is expressed as:

$$q_1(x, y, t) = (\bar{q} + q_f)(\bar{x}_c + XE)|_1,$$

with $E = e^{i(ky-\omega t)}$. At first order, the mean quantities become:

$$\bar{q}(\bar{x}_c + XE)|_1 = \bar{q}_1(\bar{x}_c) + \frac{\partial \bar{q}_1}{\partial x}(\bar{x}_c) XE,$$

$\partial \bar{q}_1/\partial x(\bar{x}_c)$ is the right derivative of $\bar{q}_1$ with respect to x calculated in $\bar{x}_c$ (it is sometimes denoted as $\partial \bar{q}_1/\partial x(\bar{x}_c^+)$) as well as $\partial \bar{q}_0/\partial x(\bar{x}_c)$ is the left derivative of $\bar{q}_0$ in $\bar{x}_c$ (denoted as $\partial \bar{q}_0/\partial x(\bar{x}_c^-)$). Finally, q_1 is written as:

$$q_1(x, y, t) = \bar{q}_1(\bar{x}_c) + \frac{\partial \bar{q}_1}{\partial x}(\bar{x}_c) XE + q_1(\bar{x}_c) E.$$

As demonstrated in section III.4.1, there is no fluctuation upstream of the shock. Thus q_0 simply reduces to:

$$q_0(x, y, t) = \bar{q}_0(\bar{x}_c) + \frac{\partial \bar{q}_0}{\partial x}(\bar{x}_c) XE.$$

Finally, the linearized Rankine-Hugoniot relations lead to an algebraic system of equations:

$$\mathbf{A}\mathbf{Z}(\bar{x}_c) = X\xi,$$

$\mathbf{Z}(\bar{x}_c)$ is the vector of the fluctuating amplitudes calculated at $\bar{x}_c \cdot \xi$ is a complex vector and $\mathbf{A}$ is a fourth-order complex matrix, which depends only on the downstream flow. The analytical expressions of these quantities are given in the appendix; *see* (A3) and (A4). The determinant of matrix $\mathbf{A}$ is different from zero, so matrix $\mathbf{A}$ can be inverted. Finally, vector $\mathbf{Z}$ at the mean shock position is known:

$$\mathbf{Z}(\bar{x}_c) = \mathbf{A}^{-1} X\xi. \tag{19}$$

Its components are given in appendix (A5). From equation (19), it is clear that the fluctuation will be « scaled » by the shock oscillation amplitude X, which cannot be determined by a linear stability analysis. At the end of any stability analysis, all fluctuating quantities are determined uniquely but with an arbitrary scaling factor. For the present problem, this property remains true even for the shock oscillation amplitude.

III.4.3 – *Final form of the stability problem*

The stability problem has been easily solved in the supersonic zone. It remains to be solved in the subsonic zone. The system of differential equations (15) can be expressed as:

$$\frac{d\mathbf{Z}}{dx} = \mathbf{C}^{-1}\mathbf{B}\mathbf{Z}, \tag{20}$$

for $x > \bar{x}_c$. This system is associated with the boundary conditions (16) and (17).

Again, this problem appears to be an eigenvalue problem: there is the trivial solution $\mathbf{Z} \equiv 0$, $X = 0$. A non-zero solution can exist only if the problem is singular, which implies a particular choice of the values of the wave number k and the complex circular frequency ω of the perturbation. This choice corresponds to a dispersion relation between these numbers, which cannot be determined analytically. Numerical integration is unavoidable.

III.5 – Numerical approach

The fourth-order linear problem (20) has a solution in a four-dimensional vector space. The solution therefore has the following form:

$$\mathbf{Z}(x) = \sum_{j=1}^{4} c_j \mathbf{Z}_j(x), \tag{21}$$

where the four c_j coefficients are unknown integration constants, which will be determined by the boundary conditions. This decomposition will be used in the remaining part of this section, which is devoted to the numerical integration of the stability problem. This integration is achieved in three steps.

The first step consists in remarking that the mean flow, at a distance from the shock, does not depend on x. In this « uniform zone », for $x \geq x_u$, an analytical solution of (20) can be calculated:

$$\mathbf{Z}(x) = \sum_{j=1}^{4} c_j \mathbf{V}_j \cdot e^{l_j x}, \tag{22}$$

where l_j and $\mathbf{V}_j$ are the eigenvalues and eigenvectors of matrix $\mathbf{C}^{-1}\mathbf{B}$ respectively (*see* Appendix A6 and A7). A more detailed analysis of this uniform zone shows that $\mathfrak{Re}(l_j) > 0$ for $j = 1$ (only). Since an exponentially increasing behaviour of $\mathbf{V}_1 \cdot \exp(l_1 x)$ is not acceptable with respect to boundary condition (17), the relation $c_1 = 0$ must be imposed. The general solution of (20) then reduces to:

$$\mathbf{Z}(x) = \sum_{j=2}^{4} c_j \mathbf{Z}_j(x). \tag{23}$$

In the second step, equation (20) is numerically integrated for each vector $\mathbf{Z}_j$ (j being 2, 3 and 4) by decreasing values of x from the $\bar{x}_u$ of the uniform zone up to the mean shock position $\bar{x}_c$. The constraint is to require the perturbation to remain in the three-dimensional vector subspace generated by $\mathbf{Z}_2$, $\mathbf{Z}_3$ and $\mathbf{Z}_4$. But the computation shows $\|\mathbf{Z}_2\| \ll \|\mathbf{Z}_3\|, \|\mathbf{Z}_4\|$, so that the subspace becomes numerically two-dimensional. To avoid this problem, an orthonormalisation of the Gram-Schmidt type has been used as in the boundary layer stability problem, *see* [10]. Finally, vectors $\mathbf{Z}_2$, $\mathbf{Z}_3$ and $\mathbf{Z}_4$ are determined up to the mean shock.

The third step is devoted to the mean shock position $\bar{x}_c$. In effect, in this position, there are two formulations of $\mathbf{Z}(x)$; the first one comes from (23) and the numerical integration of $\mathbf{Z}_2$, $\mathbf{Z}_3$ and $\mathbf{Z}_4$, and the second one is simply the boundary condition (19). These two formulations must coincide:

$$\mathbf{Z}(\bar{x}_c) = c_2 \mathbf{Z}_2(\bar{x}_c) + c_3 \mathbf{Z}_3(\bar{x}_c) + c_4 \mathbf{Z}_4(\bar{x}_c). \tag{24}$$

For a given circular frequency ω_r, the unknowns are the complex constants c_2, c_3 and c_4 and the eigenvalues (λ, ω_i). These eight real constants

correspond to the four scalar complex relations associated with (24).

A trial and error method is used to determine the eigenvalues. An initial guess is made for (λ, ω_i), then, using the numerical procedure described, the values of $\mathbf{Z}_2(\bar{x}_c)$, $\mathbf{Z}_3(\bar{x}_c)$, $\mathbf{Z}_4(\bar{x}_c)$ and $\mathbf{Z}(\bar{x}_c)$ are calculated so that equation (24) can be written. The three first components of (24) give the values of the constants c_2, c_3 and c_4. The fourth relation (coming from the fourth component of (24)) must be satisfied if the values of (λ, ω_i) are correct. Otherwise, the whole procedure is repeated with another set of values for (λ, ω_i), modified by a classical Newton procedure until convergence is achieved.

IV – STABILITY RESULTS

IV.1 – Normalisation

In the linear stability theory, the problem is obviously linear with respect to the perturbation. According to (19) the fluctuations are proportional to the shock amplitude X. In order to be able to compare the results, a normalisation must be introduced for the amplitude functions. The fluctuating pressure at the exist section has been chosen for this normalisation. As the fluctuating pressure spectrum is not known at the exit section, uniform law is simply imposed:

$$\frac{|p_f(x_e)|}{\overline{P}(x_e, y)} = \text{const} \quad \forall \omega, \forall y. \tag{25}$$

This means that the fluctuating pressure at the exit section is given as a ratio of the mean pressure. Of course, it is also possible to normalise by setting any fluctuating quantity at any x-position. For example the stability results can be adjusted with the first point of *Figure* 3.

IV.2 – Shock motion spectrum

Figure 2 shows the experimental shock motion spectrum. It exhibits a well-defined peak at approximately 200 Hz. The spectrum calculated by the present stability theory is shown in *Figure* 7. It seems that the proposed stability theory is in good agreement with Sajben's experiment: as in the experiment, our numerical results present a peak close to 200 Hz. Some differences appear between the numerical and experimental spectra but they may be due to the experimental filtering procedure.

For this diffuser length, the numerical simulation of Liou and the experiment of Sajben seem to be in good agreement (see *Figs.* 2 and 4). Nevertheless, Liou's team seems to suggest that for this diffuser length, the mechanism causing the self-excited oscillation is dominated by the viscous convective wave. The present stability results seem to indicate a mechanism without viscosity.

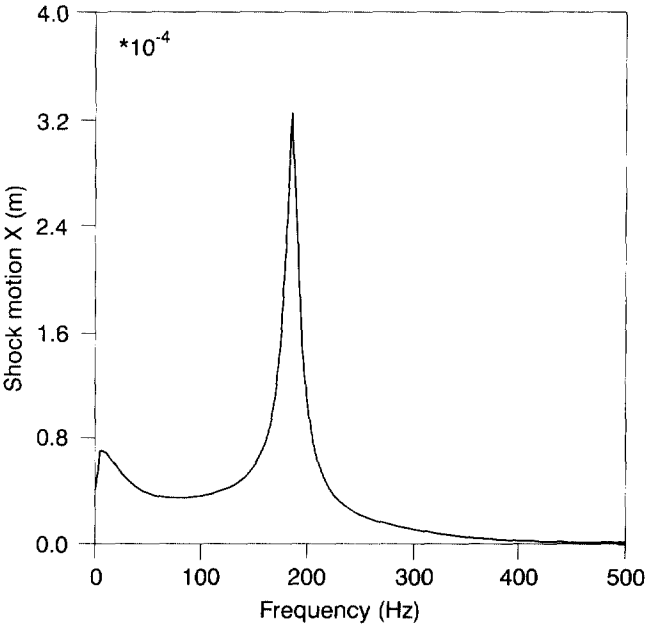

Fig. 7. – Shock motion spectrum, $l/h = 13$.

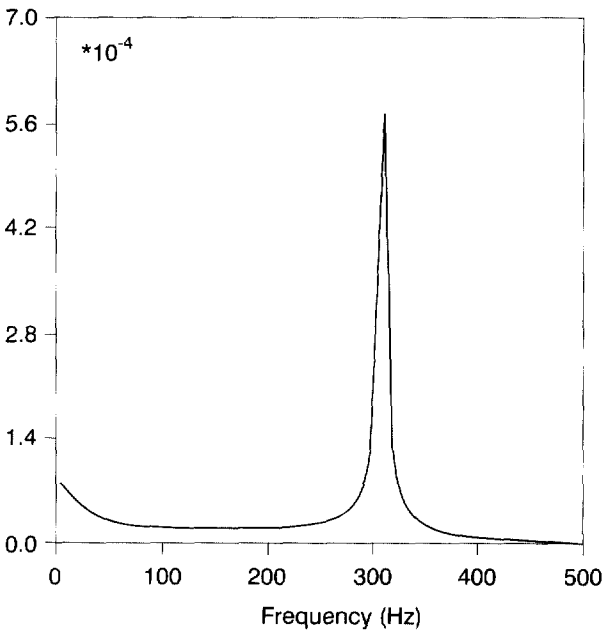

Fig. 8. – Shock motion spectrum, $l/h = 8.6$.

Concerning approximation (12), it has been proven, *see* [9], that the result of *Figure* 7 is nearly independent of y, as expected. The results presented have been obtained for a fixed value of y, but other values have been tested and presented in [9], and the results are nearly independent of y in the core region. For a diffuser length $l = 8.6\,h$, the numerical simulations of Liou show a shock motion spectrum presenting a well-defined peak at 300 Hz. Reducing

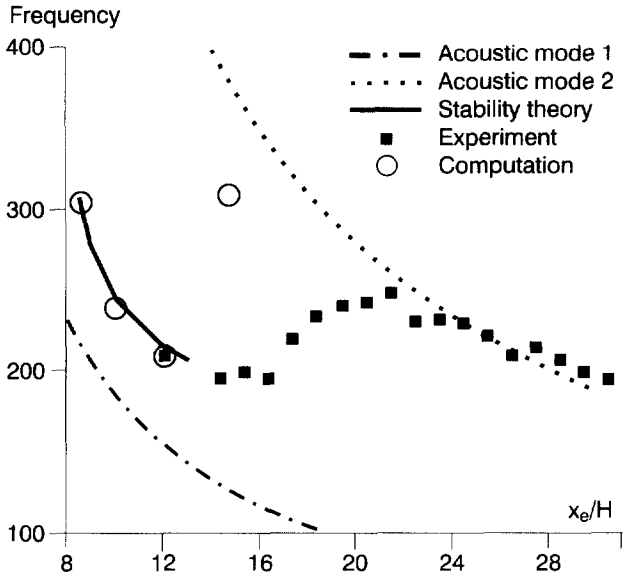

Fig. 9. – Frequency versus location of downstream boundary.

the diffuser length, the inviscid stability theory also gives a peak at 300 Hz as indicated in *Figure* 8.

The frequency variation as a function of the diffuser length is shown in *Figure* 9. The results given in [7] are shown and the stability results have been added. For a diffuser length less than or equal to $l/h = 13$, the stability theory seems to be in good agreement with the experimental and numerical results. But the present stability analysis seems to show a different physical mechanism (inviscid mechanism) from the explanations given in [7].

At this point, it is important to note that a simple acoustic analysis (as given in [3]) cannot predict the most amplified frequencies at least for $l/h \leq 13$. Furthermore, from *Figure* 9, it is clear that the peak of the shock motion spectra is strongly dependent on the diffuser length. The present linear stability analysis, limited to the core region, seems to provide good results for $l/h \leq 13$. For longer lengths, the two boundary layers collapse together upstream of the exit section and a completely different mechanism may be then responsible for the shock oscillations.

Like [7], we believe that there are two different mechanisms, depending on the diffuser length. But, contrary to [7], we fell that the shock oscillation can be explained by inviscid fluctuations. However, it is very clear these inviscid fluctuations are not pure acoustic modes (the frequencies do not coincide). The linearised shock equations must therefore play a non-negligible role as they are taken into account in the present approach.

IV.3 – Variation of ω_i with the frequency

An important result of the linear stability theory provided by the implicit dispersion relation is the value of the temporal amplification growth rate ω_i (and the value of the wave number k). The following *Table* 1 gives these values for the most sensitive frequency corresponding to the two lengths of the diffuser (see *Figs.* 7 and 8).

Table 1. – Numerical stability results.

Frequency (Hz)	$k\,(m^{-1})$	$\omega_i/2\pi$
200 Hz, $x/h = 13$	+ 4.7379	- 99.22
	- 4.853	- 99.36
300 Hz, $x/h = 8.6$	+ 4.603	- 110.98
	- 4.129	- 108.99

For this frequency range, two values of k are found. There is nothing surprising about this because if the configuration were perfectly one-dimensional, with $\bar{V}$ exactly equal to zero, there would be no preferred direction on the y axis, and k and $-k$ would be solutions of the stability problem. In our case $\bar{V}$ is not exactly equal to zero and the symmetry is only weakly broken.

The wave number k is very low so the perturbation is quasi-mono-dimensional as proposed by Culick and Rogers [11].

Furthermore, the coefficient of temporal amplification ω_i is always negative, as shown in *Figure* 10. Therefore, according to the stability definition, the mean flow is stable.

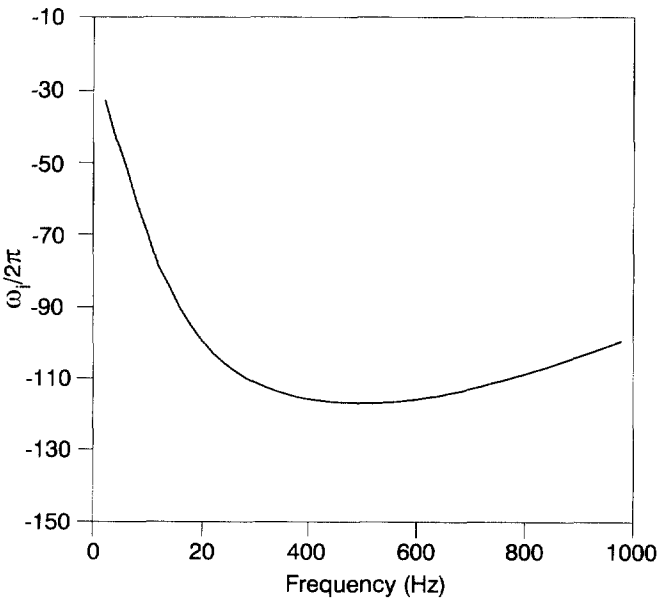

Fig. 10. – Variation of ω_i.

Thus, if the flow is strictly unperturbed (no pressure fluctuation at the exit), no shock oscillation and no perturbation in the downstream zone ust be observed. This conclusion can be tested by numerical simulation.

IV.4 – Pressure fluctuation

This section is devoted to the comparison between Sajben's experimental results, Liou's numerical results and the temporal stability results for the amplitude and phase of the pressure fluctuation. The stability results are illustrated in *Figures* 11 and 12.

To make the comparison easier, the scales are the same as Sajben's and Liou's (see *Fig.* 3). As the stability theory gives the results within an arbitrary complex factor, our results are adjusted with the first experimental point (see *Fig.* 3) of fluctuating pressure amplitude.

These results seem to agree with the experimental ones, and are at least closer to these than Liou's numerical results. The amplitude calculated by the present approach seems smaller than the experimental amplitude. In particular the latter remains constant downstream of the position $x/h = 4$, whereas the amplitude in *Figure* 11 decreases rather weakly. The amplitude in *Figure* 11 corresponds to the single frequency $f = 200$ Hz, though, whereas the experimental amplitude in *Figure* 3 covers a large frequency band.

On the other hand, concerning the phase variation (*Fig.* 12), there is very good agreement between stability results and the experimental data. It is important to note that this result has been obtained for a negative frequency, which corresponds to an upstream travelling wave. This means that the wave does not reflect on the shock.

The problem of wave reflection by a shock has been studied in detail by Culik and Rogers in [11]. With their notations, the reflection coefficient $|\beta|$ is equal to 0.18 in our case. It corresponds to an incident wave which is weakly reflected by the shock. Only low frequencies (below 40 Hz) are reflected. This is in agreement with the proposed conclusion of the previous paragraph.

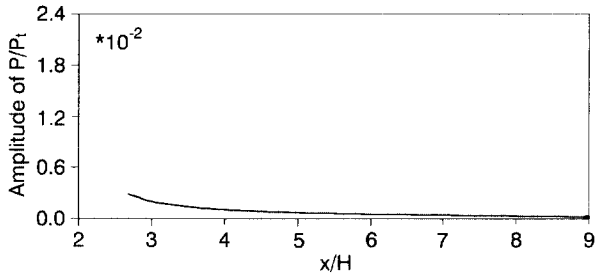

Fig. 11. – Fluctuating pressure: amplitude.

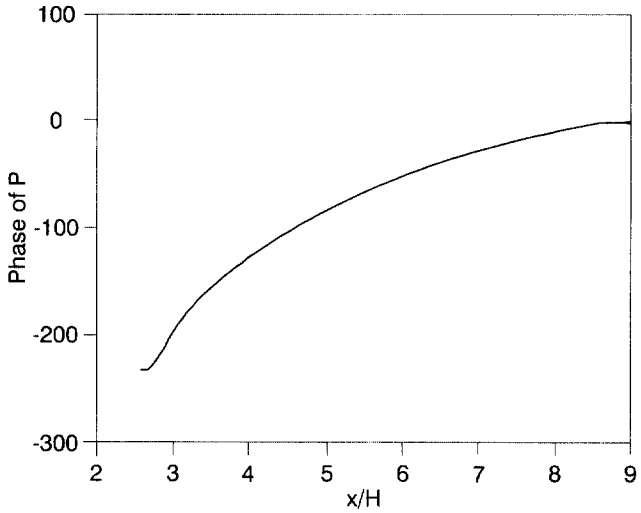

Fig. 12. – Fluctuating pressure: phase.

V – CONCLUSION

The goal of this paper is to present a new approach based on the linear stability theory to explain and predict the shock oscillations observed in some transonic diffusers. The comparisons between experimental data, numerical simulations and the linear stability analysis of self-excited oscillations can be summarised as follows:

• The temporal stability theory seems to predict some physical characteristics of the flow. The computation of the shock motion spectrum by the stability theory is in agreement with the experimental results of Sajben. Our computations give the same frequency (200 Hz) as the experiment ($l/h = 13$) and the same frequencies as the numerical simulations for $l/h = 13$.

• Our analysis shows that the mean flow is always linearly stable.

• The comparison between our theory and experiment for the fluctuating pressure shows reasonable agreement. In effect, the phase variation is very well reproduced for an upstream travelling wave.

Finally, this new study can give some insight into the physical origin of the observed self-excited shock oscillations. Furthermore it is interesting to note that this study can be generalised to the problem of buffeting.

APPENDIX

To simplify the notations the following quantities Ω and $\tilde{\omega}$ are introduced:

$$\Omega = \sqrt{k^2\,[a^2 - (\overline{U}^2 + \overline{V}^2)] + 2\,k\,\omega\,\overline{V} - \omega^2}$$

$$\tilde{\omega} = \omega - k\,\overline{V}.$$

The matrix expressions of differential system (15) are:

$$\mathbf{C} = \begin{bmatrix} 0 & \overline{\mathbf{U}} & \overline{\rho} & 0 \\ r\,\overline{\rho} & r\,\overline{T} & \overline{\rho}\,\overline{U} & 0 \\ 0 & 0 & 0 & \overline{\rho}\,\overline{U} \\ C_p\,\overline{\rho}\,\overline{U} & 0 & \overline{\rho}\,\overline{U}^2 & \overline{\rho}\,\overline{U}\,\overline{V} \end{bmatrix} \tag{A1}$$

$$\mathbf{B} = \begin{bmatrix} 0 & i\tilde{\omega} - \dfrac{\partial \overline{U}}{\partial x} & -\dfrac{\partial \overline{\rho}}{\partial x} & -ik\,\overline{\rho} \\ -r\,\dfrac{\partial \overline{\rho}}{\partial x} & -\overline{U}\,\dfrac{\partial \overline{U}}{\partial x} - r\,\dfrac{\partial \overline{T}}{\partial x} & \left(i\tilde{\omega} - \dfrac{\partial \overline{U}}{\partial x}\right)\overline{\rho} & 0 \\ ikr\,\overline{\rho} & -\overline{U}\,\dfrac{\partial \overline{U}}{\partial x} - ikr\,\overline{T} & -\overline{\rho}\,\dfrac{\partial \overline{V}}{\partial x} & \overline{\rho}\,i\tilde{\omega} \\ i\tilde{\omega}\,C_p\,\overline{\rho} - i\,\omega\,r\,\overline{\rho} & -i\,\omega\,r\,\overline{T} & \left(i\tilde{\omega} - \dfrac{\partial \overline{U}}{\partial x}\right)\overline{\rho}\,\overline{U} & i\tilde{\omega}\,\overline{\rho}\,\overline{V} - \overline{\rho}\,\overline{U}\,\dfrac{\partial \overline{V}}{\partial x} \end{bmatrix} \tag{A2}$$

The vector and matrix expressions of algebraic system (19) are:

$$\mathbf{A} = \begin{bmatrix} 0 & \overline{U}_1 & \overline{\rho}_1 & 0 \\ r\,\overline{\rho}_1 & \overline{U}_1^2 + r\,\overline{T}_1 & 2\,\overline{\rho}_1\,\overline{U}_1 & 0 \\ C_p & 0 & \overline{U}_1 & 0 \\ 0 & 0 & 0 & 1 \end{bmatrix} \tag{A3}$$

and

$$\xi = \xi_0 - \xi_1 \tag{A4}$$

wheree ξ_i is defined for $i = 0$ (upstream) and for $i = 1$ (downstream) by:

$$\xi_i = \begin{bmatrix} \dfrac{\partial \overline{\rho}_i}{\partial x}\,\overline{U}_i + \overline{\rho}_i\left(\dfrac{\partial \overline{U}_i}{\partial x} - ik\,\overline{V}_i + i\,\omega\right) \\ \dfrac{\partial \overline{\rho}_i}{\partial x} + \dfrac{\partial \overline{\rho}_i}{\partial x}\,\overline{U}_i^2 + 2\,\overline{\rho}_i\,\overline{U}_i\left(\dfrac{\partial \overline{U}_i}{\partial x} - ik\,\overline{V}_i + i\,\omega\right) \\ C_p\,\dfrac{\partial \overline{T}_i}{\partial x} + \overline{U}_i\left(\dfrac{\partial \overline{U}_i}{\partial x} - ik\,\overline{V}_i + i\,\omega\right) \\ \dfrac{\partial \overline{V}_i}{\partial x} + ik\,\overline{U}_i \end{bmatrix}$$

The components of vector $\mathbf{Z}$ at the mean shock position $\overline{x}_c$ are:

$$\begin{aligned} T(\overline{x}_c) &= \frac{\overline{U}_1^2\,\xi_2 - \overline{U}_1^2\,\xi_1\,(r\,\overline{T}_1 + \overline{U}_1^2) - \overline{\rho}_1\,\xi_3\,(\overline{U}_1^2 - r\,\overline{T}_1)}{C_r\,\overline{\rho}_1\,\overline{a}_1^2\,(\overline{M}_1^2 - 1)} \\ \rho(\overline{x}_c) &= \frac{2\,C_p\,\overline{U}_1\,\xi_1 + C_p\,\xi_2 - r\,\overline{\rho}_1\,\xi_3 + r\,\overline{\rho}_1\,\xi_1}{C_r\,\overline{a}_1^2\,(\overline{M}_1^2 - 1)} \\ u(\overline{x}_c) &= \frac{2\,C_p\,\overline{U}_1^2\,\xi_1 - C_p\,\overline{U}_1\,\xi_2 + C_p\,r\,\overline{T}_1\,\xi_1 + \overline{U}_1\,r\,\overline{\rho}_1\,\xi_3}{C_r\,\overline{\rho}_1\,\overline{a}_1^2\,(\overline{M}_1^2 - 1)} \\ v(\overline{x}_c) &= \xi_1 \end{aligned} \tag{A5}$$

The eigenvalues of $\mathbf{C}^{-1}\,\mathbf{B}$ in the uniform zone are:

$$\left.\begin{aligned} l_1 &= \frac{-i\,\tilde{\omega}\,\overline{U} + a\,\Omega}{a^2 - \overline{U}^2} \\ l_2 &= \frac{-i\,\tilde{\omega}\,\overline{U} + a\,\Omega}{a^2 - \overline{U}^2} \\ l_3 = l_4 &= \frac{i\,\tilde{\omega}}{\overline{U}} \end{aligned}\right\} \tag{A6}$$

The last eigenvalue is of order 2. The corresponding eigenvectors of $\mathbf{C}^{-1}\,\mathbf{B}$ are:

$$\mathbf{V}_1 = \begin{bmatrix} \dfrac{1}{C_p\,k}\left(\dfrac{\tilde{\omega}\,\overline{U}^2 + i\,\overline{U}\,a\,\Omega}{a^2 - \overline{U}^2} + \tilde{\omega}\right) \\ \dfrac{\overline{\rho}}{ka^2}\left(\dfrac{\tilde{\omega}\,\overline{U}^2 + i\,\overline{U}\,a\,\Omega}{a^2 - \overline{U}^2} + \tilde{\omega}\right) \\ -\dfrac{1}{k\,\overline{U}}\left(\dfrac{\tilde{\omega}\,\overline{U}^2 + i\,\overline{U}\,a\,\Omega}{a^2 - \overline{U}^2} + \tilde{\omega}\right) \\ 1 \end{bmatrix} \tag{A7-a}$$

$$\mathbf{V}_2 = \begin{bmatrix} \dfrac{1}{C_p\,k}\left(\dfrac{\tilde{\omega}\,\overline{U}^2 - i\,\overline{U}\,a\,\Omega}{a^2 - \overline{U}^2} + \tilde{\omega}\right) \\ \dfrac{\overline{\rho}}{ka^2}\left(\dfrac{\tilde{\omega}\,\overline{U}^2 - i\,\overline{U}\,a\,\Omega}{a^2 - \overline{U}^2} + \tilde{\omega}\right) \\ -\dfrac{1}{k\,\overline{U}}\left(\dfrac{\tilde{\omega}\,\overline{U}^2 - i\,\overline{U}\,a\,\Omega}{a^2 - \overline{U}^2} + \tilde{\omega}\right) \\ 1 \end{bmatrix} \tag{A7-b}$$

For the double eigenvalue, the eigen subspace is two-dimensional and is generated by:

$$\mathbf{V}_3 = \begin{bmatrix} 1 \\ -\dfrac{\overline{\rho}}{\overline{T}} \\ 0 \\ 0 \end{bmatrix} \quad \text{and} \quad \mathbf{V}_4 = \begin{bmatrix} 0 \\ 0 \\ 1 \\ \dfrac{-\tilde{\omega}}{k\,\overline{U}} \end{bmatrix} \tag{A7-c}$$

REFERENCES

[1] Cambier L., Darracq D., Gazaix M., Guillen Ph., Jouet Ch., Le Toullec L. – Améliorations récentes du code d'écoulements compressibles FLU3M, Progress and Challenges in CFD Methods and Algorithms, *AGARD-CP-578*, April 1996.

[2] Bogar T. J., Sajben M., Kroutil J. C. – Characteristic Frequencies of Transonic Diffuser Flow Oscillations, *AIAA Journal*, Sept. 1983, **21**, 1232-1240.

[3] Bogar T. J. – Structure of Self-Excited Oscillations in Transonic Diffuser Flows, *AIAA Journal*, Jan. 1986, **24**, 54-61.

[4] Salmon J. T., Bogar T. J., Sajben M. – Laser Doppler Velocimeter Measurements in Unsteady, Separated, Transonic Diffuser Flows, *AIAA Journal*, Dec., **21**, 1690-1697.

[5] Liou M. S., Coakley T. J. – Numerical Simulations of Unsteady Transonic Flow in Diffuser, *AIAA Journal*, Aug., **22**, 1139-1144.

[6] Liou M. S., Coakley T. J., Bergmann M. Y. – Numerical Simulation of Transonic Flow in Diffusers, *AIAA Paper n° 81-1240*, 1981.

[7] Coakley T. J., Hsieh T. – Downstream Boundary Effects on the Frequency of Self-Excied Oscillations in Transonic Diffuser Flow, *AIAA Paper n° 87-0167*, Jan. 1987,.

[8] Hsieh T., Bogar T. J., Coakley T. J. – Numerical Simulation and Comparison for Self-Excited Oscillations in Diffuser Flow, *AIAA Journal*, July 1987, **25**, 936-943.

[9] Casalis G., Hallard R., Jouet Ch., Robinet J.-Ch. – Calcul des caractéristiques stationnaires et instationnaires d'un écoulement décollé dans une tuyère. Cas bidimensionnel, *93/CNES/3040, Rapport Technique*, Sept. 1996.

[10] Habiballah M. – Analyse de l'instabilité des couches limites laminaires et prévisions de la transition du régime laminaire au régime turbulent, *Thèse ENSAE*, 1981.

[11] Culick F. E. C., Rogers T. – The Response of Normal Shocks in Diffusers, *AIAA Journal*, **21**, Oct. 1983, 1382-1390.

Acknowledgments. – This study has been carried out under contract n° 93/CNES/3040 granted by the French Centre National d'Études Spatiales (CNES). The mean flow has been computedd by Ch. Jouet and R. Hallard. This article is dedicated to the memory of Ch. Jouet.